Numerical method for determination of the NMR frequency of the single-qubit operation in a silicon-based solid-state quantum computer

H. T. Hui
School of Information Technology and Electrical Engineering, University of Queensland, QLD 4072, Australia
(Received 31 May 2006; revised manuscript received 18 September 2006; published 8 November 2006)

A numerical method is introduced to determine the nuclear magnetic resonance frequency of a donor (^{31}P) doped inside a silicon substrate under the influence of an applied electric field. This phosphorus donor has been suggested for operation as a qubit for the realization of a solid-state scalable quantum computer. The operation of the qubit is achieved by a combination of the rotation of the phosphorus nuclear spin through a globally applied magnetic field and the selection of the phosphorus nucleus through a locally applied electric field. To realize the selection function, it is required to know the relationship between the applied electric field and the change of the nuclear magnetic resonance frequency of phosphorus. In this study, based on the wave functions obtained by the effective-mass theory, we introduce an empirical correction factor to the wave functions at the donor nucleus. Using the corrected wave functions, we formulate a first-order perturbation theory for the perturbed system under the influence of an electric field. In order to calculate the potential distributions inside the silicon and the silicon dioxide layers due to the applied electric field, we use the multilayered Green's functions and solve an integral equation by the moment method. This enables us to consider more realistic, arbitrary shape, and three-dimensional qubit structures. With the calculation of the potential distributions, we have investigated the effects of the thicknesses of silicon and silicon dioxide layers, the relative position of the donor, and the applied electric field on the nuclear magnetic resonance frequency of the donor.

DOI: 10.1103/PhysRevB.74.195309 PACS number(s): 03.67.Lx, 76.60.−k, 85.30.De, 31.15.Md

I. INTRODUCTION

Quantum computers have been proposed to possess enormous computation power over conventional computers for certain types of problems.[1] Since then, a large amount of research interest has been found in the realization and design of quantum computers.[2–9] Recently, the realization of quantum computers by solid-state materials has gained considerable attention because of the possibility of designing scalable quantum computers. Proposals have been found on realizing the qubit (the basic operation unit in a quantum computer) using nuclear spins in atoms[4–6] and electron spins in quantum dots.[7] In 1998, Kane[4] proposed to use the nuclear spin of a phosphorus atom (^{31}P) embedded in a silicon substrate as a qubit for quantum computing. In Kane's original idea, the operation of the qubit is achieved by a combination of the rotation of the phosphorus nuclear spin through a globally applied magnetic field and the selection of the phosphorus nucleus through a locally applied electric field. The local electric field is applied through a metallic gate, called the *A* gate, which is a metallic strip laid on top of the silicon substrate. As the magnetic field is applied globally, all the phosphorus nuclei (qubits) in the quantum computer will be affected. Hence it is important to be able to bring only a specific phosphorus nucleus into magnetic resonance with the magnetic field, i.e., the addressing function. This addressing function is accomplished by applying a voltage to the *A* gate to change the nuclear magnetic resonance (NMR) frequency of the phosphorus nucleus. The applied voltage changes the hyperfine interaction between the phosphorus nucleus and the outer valence electron. This in turn changes the magnetic resonance frequency of the nucleus. Therefore it is important to know the relationship between the applied voltage on the *A* gate and the change of the NMR frequency. To obtain this relationship is actually divided into two problems. The first is to obtain the wave functions of the donor electron, and the second is to determine the potential distribution inside the silicon substrate. Research on the first problem started several decades ago from Kohn and Luttinger's effective-mass theory.[10–13] In order to obtain the correct value of the wave function at the donor nucleus, Kohn[13] introduced a "central-cell correction" technique. Subsequent modifications[14–17] to the effective-mass theory have greatly improved its accuracy in calculating the energy levels. However, to obtain the accurate values of the wave functions at the donor nucleus still posed a challenging problem. To tackle the second problem, several attempts have been reported in the literature.[4,18–20] Kane[4] obtained the potential distribution due to the voltage on the *A* gate and its relationship to the nuclear magnetic resonance frequency by following estimates of Kohn of shallow donor Stark shifts in silicon.[13] Larionov *et al.*[18] considered simplified *A* gate geometries and obtained an analytical expression for the potential function. Kettle *et al.*[19] used a computer-aided design (CAD) tool to model the qubit structure as a two-dimensional (2D) device and Koiller *et al.*[20] considered a uniform potential distribution.

In this study, we will address both these problems. To tackle the first problem, we introduce an empirical *correction factor* to the wave functions obtained by Ning and Sah[16] at the donor nucleus. This correction factor accounts for the rapid fluctuation of the wave functions from their (*averaged*) values at the donor nucleus predicted by the effective-mass theory. To tackle the second problem, we use the multilayered Green's functions and solved an integral equation by the moment method.[21] We use the complex image method[22] to calculate the spatial domain Green's functions from the spectral domain multilayered Green's functions, and this enables us to consider more realistic, arbitrary shape, and three-dimensional (3D) structured *A* gates. Using the corrected

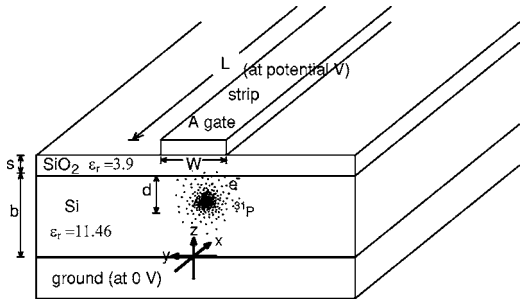

FIG. 1. The single-qubit structure of the silicon-based solid-state quantum computer proposed by Kane (Ref. 4).

wave functions and the numerical values of potential distribution, we are able to formulate a first-order perturbation theory for the perturbed system under the influence of an electric field. Results obtained on the change of the NMR frequency due to the applied voltage on the A gate will be compared with those obtained by previous approximation methods.

II. FIRST-ORDER PERTURBATION THEORY FOR THE DONOR ELECTRON WAVE FUNCTION UNDER THE INFLUENCE OF THE GATE VOLTAGE

Consider the structure of the single qubit proposed by Kane[4] as shown in Fig. 1. It is a phosphorus atom (isotope ^{31}P) doped in a silicon substrate (isotope ^{28}Si). On top of the silicon substrate is an insulating layer of silicon dioxide. Below the silicon substrate is a grounding layer at 0 potential. On top of the silicon dioxide layer is a metallic strip, called the A gate, with a control voltage V. The electron cloud of the phosphorus atom can be drifted by applying a voltage on the A gate. The drift of the electron cloud can change the hyperfine interaction between the phosphorus nucleus and the outermost valence electron, and hence can change the nuclear magnetic resonance frequency of phosphorus. The Hamiltonian equation for the electron wave function is given by

$$H\Psi' = E'\Psi', \tag{1}$$

where the total Hamiltonian H is

$$H = H_0 + H_V = H_0 + eV. \tag{2}$$

In Eq. (2), H_0 is the Hamiltonian of the donor (phosphorus ^{31}P) electron inside the silicon substrate, H_V is the additional electron Hamiltonian due to the potential V excited by the voltage on the A gate, and e is the electron charge. Larionov *et al.*[18] has attempted to solve Eq. (2) by using the perturbation theory under idealistic assumptions. In the following analysis, we treat eV as a perturbation to the unperturbed system described by H_0.

A. Wave functions of the phosphorus (^{31}P) donor electron in a silicon host from the effective-mass theory

Using the effective-mass theory proposed by Kohn and Luttinger[10–13] and the subsequent modifications by several authors,[14–17] the problem of the unperturbed system, i.e., a phosphorus donor atom in the silicon host, can be solved. Particularly, the donor energy levels can be obtained accurately and the donor electron wave function can be predicted accurately outside the donor nucleus.[16] In this study, we use the results obtained by Ning and Sah[16] on the electron wave functions. But we note that although these wave functions can yield very accurate results on energy levels, they fail to indicate the strength of the hyperfine interaction between the donor electron and the phosphorus nucleus, i.e., the value of the magnitude square of the wave function at position of the phosphorus nucleus $|\Psi_{A_1}(0)|^2$, where the A_1 subscript indicates the ground state of phosphorus in silicon. Actually this value is only about 44% of the experimental value.[23,12] Hence, we need to make a modification to these wave functions at the position of the donor nucleus in order to calculate the hyperfine interaction accurately at this position. According to the effective-mass theory,[13] the electron wave functions $\Psi(\mathbf{r})$ for the unperturbed phosphorus in silicon consist of two parts, the Bloch wave function $\varphi(\mathbf{k},\mathbf{r})$ and the hydrogenic wave function $F(\mathbf{r})$. That is,

$$\Psi_{A_1}(\mathbf{r}) = \frac{1}{\sqrt{6}} F_{A_1}^{1s}(\mathbf{r})[\varphi(k_x,\mathbf{r}) + \varphi(-k_x,\mathbf{r}) + \varphi(k_y,\mathbf{r}) + \varphi(-k_y,\mathbf{r}) + \varphi(k_z,\mathbf{r}) + \varphi(-k_z,\mathbf{r})], \tag{3}$$

$$\Psi_{2s}(\mathbf{r}) = \frac{1}{\sqrt{6}} F_{2s}(\mathbf{r})[\varphi(k_x,\mathbf{r}) + \varphi(-k_x,\mathbf{r}) + \varphi(k_y,\mathbf{r}) + \varphi(-k_y,\mathbf{r}) + \varphi(k_z,\mathbf{r}) + \varphi(-k_z,\mathbf{r})], \tag{4}$$

$$\Psi_{3s}(\mathbf{r}) = \frac{1}{\sqrt{6}} F_{3s}(\mathbf{r})[\varphi(k_x,\mathbf{r}) + \varphi(-k_x,\mathbf{r}) + \varphi(k_y,\mathbf{r}) + \varphi(-k_y,\mathbf{r}) + \varphi(k_z,\mathbf{r}) + \varphi(-k_z,\mathbf{r})], \tag{5}$$

where the hydrogenic wave functions are, respectively,

$$F_{A_1}^{1s}(\mathbf{r}) = \frac{1}{\sqrt{\pi}} \left(\frac{1}{a_{A_1}}\right)^{3/2} e^{-r/a_{A_1}}, \tag{6}$$

$$F_{2s}(\mathbf{r}) = \frac{1}{4\sqrt{2\pi}} \left(\frac{1}{a^*}\right)^{3/2} \left(2 - \frac{r}{a^*}\right) e^{-r/2a^*}, \tag{7}$$

$$F_{3s}(\mathbf{r}) = \frac{1}{81\sqrt{3\pi}} \left(\frac{1}{a^*}\right)^{3/2} \left[27 - 18\frac{r}{a^*} + 2\left(\frac{r}{a^*}\right)^2\right] e^{-r/3a^*}. \tag{8}$$

The Bohr radii, a_{A_1} and a^*, in these hydrogenic wave functions were obtained by a variational method[16] to minimize the energy levels. Their values are

$$a_{A_1} = 23.1 \text{ a.u.} = 12.22 \times 10^{-10} \text{ m}, \tag{9}$$

$$a^* = 39.7 \text{ a.u.} = 21.00 \times 10^{-10} \text{ m}. \tag{10}$$

Note that we have not listed the other two $1s$ state wave functions, i.e., the $1s(E)$ and the $1s(T_2)$ states. These two states are orthogonal to the $1s(A_1)$ state by means of the Bloch wave functions associated with them, and hence they have no contribution to the first-order perturbation terms. Also we will not consider the valley-orbit splitting of the $2s$

or $3s$ state as the splitting is not of a significant type as that in the $1s$ state.[13] All the $2p$ and $3p$ wave functions have no contribution at the donor site, and hence they are not considered. We also ignore all excited states higher than $n=3$ as their contributions are negligible.

As noted by Ning and Sah,[16] the effective-mass theory is correct only outside the central-core region, i.e., for $r \geqslant R_z = 6.79 \times 10^{-11}$ m. This is due to the inability of the effective-mass theory to model the rapidly fluctuating donor potential accurately near the donor nucleus, i.e., $r < R_z$. Currently, a viable theory that can accurately predict the wave function inside the central-core region is still lacking. But in view of the accurate predictions of the energy levels and the values of the wave function outside the central-core region by the effective-mass theory, we use a correction factor c to account for the rapid fluctuation of the wave functions from their (*averaged*) values at the donor nucleus $\mathbf{r}=0$ predicted by the effective-mass theory. This correction factor is obtained by

$$c = \frac{\text{measured value of } |\Psi_{A_1}(0)|^2}{\text{value of } |\Psi_{A_1}(0)|^2 \text{ based on the effective-mass theory}} = 1.54. \tag{11}$$

We assume that this correction factor applies also to the excited states. The use of this correction factor is to be justified from a comparison with the results obtained by other methods.

B. First-order perturbation theory

With the wave functions [Eqs. (3)–(8)] of the unperturbed system H_0, we can solve Eq. (1) using the perturbation theory. We write Eq. (2) as

$$H = H_0 + \lambda W, \tag{12}$$

where $\lambda W = eV$ represents a small perturbation and

$$H_0 \Psi_n = E_n \Psi_n, \tag{13}$$

where Ψ_n and E_n are, respectively, the wave function and the energy of the n state of the unperturbed system. Consider the first-order perturbation to the ground state $\Psi_{A_1}(0)$. We obtain the ground-state wave function $\Psi'_{A_1}(0,V)$ of the perturbed system as

$$\begin{aligned}\Psi'_{A_1}(0,V) &\approx c\Psi_{A_1}(0) \\ &+ \frac{H_{V2sA_1} - H_{VA_1A_1}\langle \Psi_{2s}(\mathbf{r})|\Psi_{A_1}(\mathbf{r})\rangle}{(E_{A_1} - E_2)(1 - \langle \Psi_{A_1}(\mathbf{r})|\Psi_{2s}(\mathbf{r})\rangle\langle \Psi_{2s}(\mathbf{r})|\Psi_{A_1}(\mathbf{r})\rangle)} \\ &\times c\Psi_{2s}(0) \\ &+ \frac{H_{V3sA_1} - H_{VA_1A_1}\langle \Psi_{3s}(\mathbf{r})|\Psi_{A_1}(\mathbf{r})\rangle}{(E_{A_1} - E_3)(1 - \langle \Psi_{A_1}(\mathbf{r})|\Psi_{3s}(\mathbf{r})\rangle\langle \Psi_{3s}(\mathbf{r})|\Psi_{A_1}(\mathbf{r})\rangle)} c\Psi_{3s}(0).\end{aligned} \tag{14}$$

The various terms and symbols in Eq. (14) are given in Appendix A. Note that the $2s$ and $3s$ states are no longer orthogonal to the $1s(A_1)$ state because they use different Bohr radii [Eqs. (9) and (10)]. As shown in Appendix A, the terms $\langle \Psi_{2s}(\mathbf{r})|\Psi_{A_1}(\mathbf{r})\rangle$ and $\langle \Psi_{3s}(\mathbf{r})|\Psi_{A_1}(\mathbf{r})\rangle$ are independent of the voltage on the A gate and can be evaluated numerically. Using their numerical values and the values of the wave functions at the donor nucleus position $\Psi_{A_1}(0)$, $\Psi_{2s}(0)$, and $\Psi_{3s}(0)$, we can simplify Eq. (14) as follows:

$$\begin{aligned}|\Psi'_{A_1}(0,V)|^2 \approx{}& 4.4 \times 10^{29} + |H_{V2sA_1} - 0.71H_{VA_1A_1}|^2 1.2 \\ &\times 10^{69} \\ &+ |H_{V3sA_1} - 0.27H_{VA_1A_1}|^2 8.1 \times 10^{67} + (H_{V2sA_1} \\ &- 0.71H_{VA_1A_1}) 4.5 \times 10^{49} + (H_{V2sA_1} \\ &- 0.71H_{VA_1A_1})(H_{V3sA_1} - 0.27H_{VA_1A_1}) 6.2 \\ &\times 10^{68} + (H_{V3sA_1} - 0.27H_{VA_1A_1}) 1.2 \times 10^{49}.\end{aligned} \tag{15}$$

Once $|\Psi'_{A_1}(0,V)|^2$ is known, the hyperfine interaction constant A_h is found by[18]

$$A_h(V) = \frac{2}{3}|\Psi'_{A_1}(0,V)|^2 \mu_B g_N \mu_N \mu_0, \tag{16}$$

where μ_B is the Bohr magnetron, g_N is the nuclear g factor for ^{31}P, μ_N is the nuclear magnetron, and μ_0 is the permeability of silicon. When the donor electron is in the ground state, the NMR frequency f is given by (to the second-order accuracy)[4,19]

$$hf = 2g_N\mu_N B + 2A_h(V) + \frac{2A_h^2(V)}{\mu_B B}, \tag{17}$$

where h is the Planck's constant and B is the applied static magnetic field.

C. Calculation of the potential inside the silicon and silicon dioxide layers due to the gate voltage

To calculate the various perturbation terms in Eq. (14), we need to know the potential $V(\mathbf{r})$ due to the applied voltage at the A gate (see Appendix A). There have been several attempts[4,18–20] to calculate this potential as mentioned in the Sec. I. In our current study, we shall solve the Poisson's equation for an arbitrary 3D A gate structure using the multilayered Green's functions.[24] In order to simulate the infinitely long structure of the strip in one direction, the method we use is to first assume a finite-length strip and then vary the length until the effect of the length is negligible on the nuclear magnetic resonance frequency of the donor. The multilayered Green's functions for qubit structure shown in Fig. 1 are obtained from the work of Li *et al.*[24] and are given in Appendix B. In our numerical calculations, these Green's functions are used to formulate an integral equation which is then solved using the moment method[21] (see Appendix B).

III. RESULTS AND DISCUSSIONS

A. The potential variation

We first validate the numerical method used to calculate the potential $V(\mathbf{r})$. For this, we calculate the capacitance be-

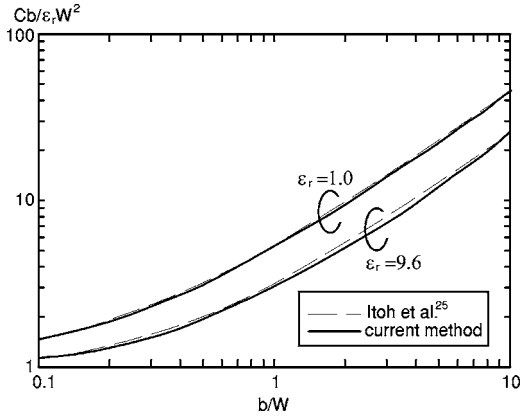

FIG. 2. Comparison of the calculated normalized capacitance of two square parallel plates by using the multilayered Green's functions and that obtained by Itoh *et al.* (Ref. 25). The square plates are with a side length of W and separation of b and separated by a dielectric medium with a dielectric constant ε_r.

tween two square parallel plates separated by a dielectric medium. The results are shown in Fig. 2 and compared with the results obtained by Itoh *et al.*[25] The square plates are with a side length W and separation b. Two cases of the dielectric constant for the dielectric medium have been calculated, $\varepsilon_r=1.0$ and $\varepsilon_r=9.6$. As can be seen, our results are in good agreement with those in the literature.

As we mentioned earlier, we model the infinitely long strip by a finite-length strip. We therefore need to know how long is the strip that approximately gives the same potential at the donor site as an infinitely long strip. We first simplify the A gate geometry to a rectangular shape with a same width as the strip and hence merged with the strip. This is the most common assumption in the previous studies[4] and we shall only consider this gate structure in all the following studies, although other gate structures can also be easily modeled by our method. Figure 3 shows the calculated potential profiles in the silicon and silicon dioxide layers along the z direction with different strip lengths. The dimensions and parameters (see Fig. 1) are $s=5$ nm, $b=60$, $W=7$ nm, ε_r of silicon $=11.46$, and ε_r of silicon dioxide$=3.9$. The potentials are obtained along a line in the z direction at $x=20$ nm and $y=0$. Three cases of strip lengths are shown: $L=35$ nm, $L=70$ nm, and $L=140$ nm. It can be seen that the potential profiles for the cases of $L=70$ nm and $L=140$ nm have little difference. Hence in the following studies, we will assume a strip length of $L=70$ nm.

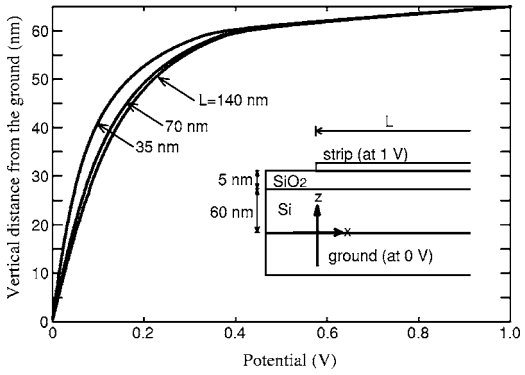

FIG. 3. Variation of the potential profile along the z direction at $x=20$ nm and $y=0$ in the silicon and silicon dioxide layers with different strip lengths. $s=5$ nm, $b=60$ nm, $W=7$ nm, ε_r of silicon $=11.46$, and ε_r of silicon dioxide$=3.9$.

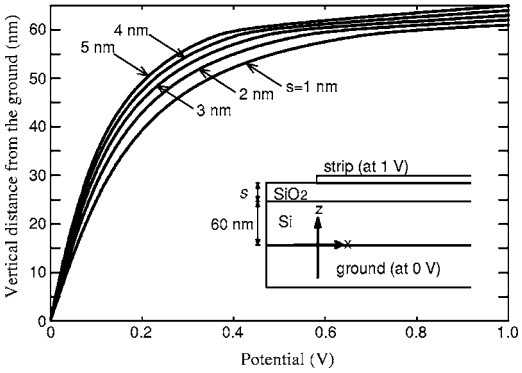

FIG. 4. Variation of the potential profile along the z direction at $x=20$ nm and $y=0$ in the silicon and silicon dioxide layers with different silicon dioxide thicknesses. $b=60$ nm, $L=70$ nm, $W=7$ nm, ε_r of silicon$=11.46$, and ε_r of silicon dioxide$=3.9$.

The choice of the silicon layer thickness of 60 nm and silicon dioxide layer thickness of 5 nm was typically reported in previous studies.[19] It was also reported that both the silicon and the silicon dioxide layer thicknesses have a significant effect on the potential profiles in these two layers. Figures 4 and 5 show the differences in potential profiles for different silicon dioxide and silicon layer thicknesses. The potential profiles are obtained along the z direction at $x=20$ nm and $y=0$. From Fig. 4, it can be seen that with a silicon layer thickness of 60 nm, the potential profiles for different silicon dioxide layer thicknesses are very different. Assuming the donor site is at $x=20$ nm, $y=0$, and $z=40$ nm in the silicon layer, the difference of potential at the donor site for silicon dioxide layer thickness of 5 nm and 1 nm is about 0.08 V. This is quite significant as the potential for the 5 nm case is only about 0.13 V while the potential for the 1 nm case is about 0.21 V. Furthermore, with a silicon dioxide layer thickness of 1 nm, the potential dropped across the silicon layer is about 80% of the gate voltage. However, when the silicon dioxide layer is 5 nm, the potential dropped across the silicon layer is only about 40% of the

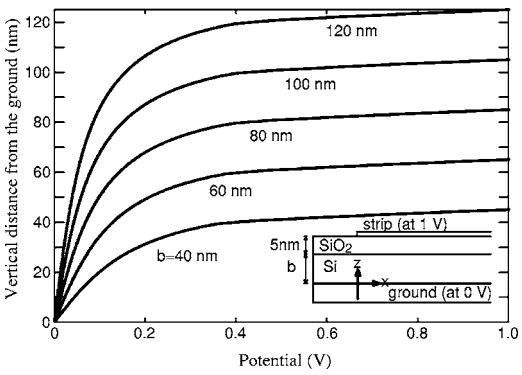

FIG. 5. Variation of the potential profile along the z direction at $x=20$ nm and $y=0$ in the silicon and silicon dioxide layers with different silicon thicknesses. $s=5$ nm, $L=70$ nm, $W=7$ nm, ε_r of silicon$=11.46$, and ε_r of silicon dioxide$=3.9$.

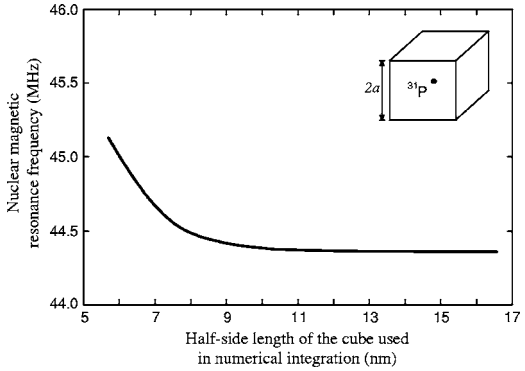

FIG. 6. Convergence of the nuclear magnetic resonance frequency with respect to the cube size used in the numerical calculation to obtain the perturbation terms. The donor site is at $x=20$ nm, $y=0$, and $z=40$ nm. $s=5$ nm, $b=60$ nm, $L=70$ nm, $W=7$ nm, ε_r of silicon=11.46, ε_r of silicon dioxide=3.9, and the applied static magnetic field $B=2$ T.

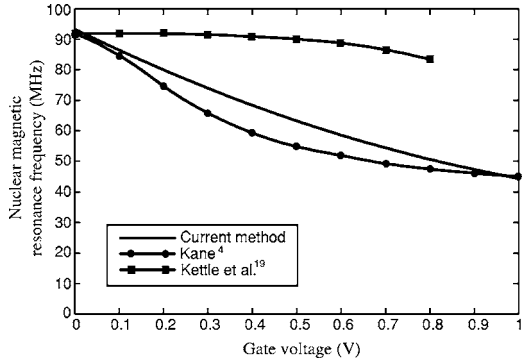

FIG. 7. The change of the nuclear magnetic resonance frequency with the gate voltage. The donor site is at $x=20$ nm, $y=0$, and $z=40$ nm and the applied static magnetic field $B=2$ T. $s=5$ nm, $b=60$ nm, $L=70$ nm, $W=7$ nm, ε_r of silicon=11.46, and ε_r of silicon dioxide=3.9.

gate voltage. However, fabrication of a 1 nm silicon dioxide layer on top of a silicon substrate is more challenging than a 5 nm one.[26] On the other hand, when changing the silicon layer thickness, the difference of the potential in the donor site is not as significant as changing the silicon dioxide layer thickness. Assuming the donor site is at $x=20$ nm, $y=0$, and is 20 nm from the silicon dioxide interface in the z direction. From the results shown in Fig. 5, with a silicon dioxide layer thickness of 5 nm, the difference in potential at the donor site with a silicon layer thickness of 40 nm and 120 nm is about 0.06 V while the potential at the donor site with a silicon layer thickness of 120 nm is about 0.16 V. Hence the change of potential from 120 nm to 40 nm is about 38%.

B. The NMR frequency

Now we use Eqs. (15)–(17) to determine the NMR frequency f of the donor under the influence of the gate voltage. We first evaluate the various perturbation terms in Eq. (15), i.e., $H_{VA_1A_1}$, H_{V2sA_1}, and H_{V3sA_1}. As shown in Appendix A, these three terms can be calculated numerically. In the numerical calculation of these terms [see Eqs. (A1)–(A3) in Appendix A], we assume the integration volume V_0 to be a finite cube centered on the donor nucleus. We find that the volume of this cube can be much smaller than the silicon substrate. Figure 6 shows the convergence of the nuclear magnetic resonance frequency f with respect to the cube size. The donor site is at $x=20$ nm, $y=0$, and $z=40$ nm. The other dimensions and parameters are $s=5$ nm, $b=60$ nm, $L=70$ nm, $W=7$ nm, ε_r of silicon=11.46, ε_r of silicon dioxide=3.9, and the applied static magnetic field $B=2$ T. As seen from Fig. 6, convergence is achieved at about $a=11$ nm, where a is the half-side length of the cube. Hence, we will use a cube size with a half-side length of 13.85 nm in the subsequent studies (compared with the length of a unit cell of silicon of 0.543 nm). With this cube size, the NMR frequency is found to be $f=44.4$ MHz.

Figure 7 shows the change of the NMR frequency f with the gate voltage. The donor site is at the same position as in Fig. 6 and all other dimensions and parameters are also the same. The results obtained by Kane[4] and Kettle *et al.*[19] have also been shown in Fig. 7 for comparison. Kane's result was obtained by following estimates of Kohn of shallow donor Stark shifts in silicon[13] while the result of Kettle *et al.* was obtained based on computer simulation of a 2D structure. It can be seen that our result shows a much greater hyperfine interaction than that of Kettle *et al.* but a slightly smaller hyperfine interaction than Kane's result. Note that our result is very close to Kane's result near 0 V and 1 V.

As shown earlier, the thicknesses of the silicon and silicon dioxide layers have a quite significant effect on the potential at the donor site. Here we further investigate the effect on the NMR frequency. As shown in Fig. 8, we see that the effect on the NMR frequency is indeed quite significant. The resonance frequency (the curve referring to the left vertical axis) changes from 36.6 MHz when thickness of the silicon dioxide layer is 1 nm to 44.4 MHz when the thickness is 5 nm. On the other hand, when the thickness of the silicon layer is 40 nm, the resonance frequency is 51.5 MHz (the curve re-

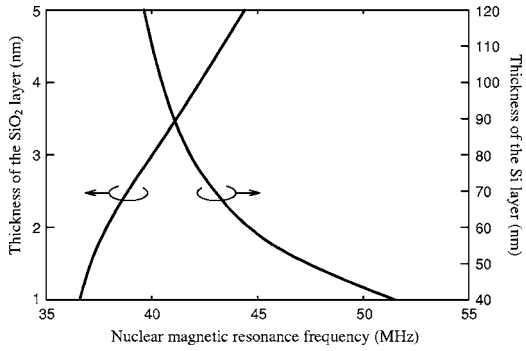

FIG. 8. The variations of the nuclear magnetic resonance frequency with the thicknesses of the silicon (Si) and silicon dioxide (SiO_2) layers. For the variation of the thickness of the silicon layer, the thickness of the silicon dioxide layer is fixed at $s=5$ nm, and the donor site is at $x=20$, $y=0$, and z being 20 nm from the Si/SiO_2 interface. For the variation of the thickness of the silicon dioxide layer, the thickness of the silicon layer is fixed at $b=60$ nm, and the donor site is at $x=20$, $y=0$, and $z=40$ nm. The applied static magnetic field $B=2$ T and the other dimensions and parameters are $L=70$ nm, $W=7$ nm, ε_r of silicon=11.46, ε_r of silicon dioxide=3.9.

ferring to the right vertical axis). But when the thickness of the silicon layer is increased to 120 nm, the resonance frequency is reduced to 39.6 MHz. Hence a thinner silicon dioxide layer and a thicker silicon layer will tend to increase the hyperfine interaction and result in a greater control on the NMR frequency.

Finally, we study the effect of misplacing the donor at a slightly different position from its default position at $x=20$ nm, $y=0$, and $z=40$ nm (see Fig. 1 for the position of the coordinate system). The dimensions and parameters of the qubit structure are $s=5$ nm, $b=60$ nm, $L=70$ nm, $W=7$ nm, ε_r of silicon=11.46, ε_r of silicon dioxide=3.9, and the applied static magnetic field $B=2$ T. The results are shown in Fig. 9. When varying the donor site along the x axis, we fix the y and z coordinates of the donor are at 0 and 40 nm, respectively. It can be seen (the curve referring to the left vertical axis) that the change in resonance frequency is quite significant when the donor moves closer to the open end ($x=0$). The change in resonance frequency with the donor at $x=20$ nm and $x=0$ is about 19%. Next we vary the donor site along the y axis the x and z coordinates of the donor site fixed at 20 and 40 nm, respectively. The result (the curve referring to the right vertical axis) demonstrates a limitation to the placement of adjacent single qubits. We see that the difference in resonance frequency with the donor site at $y=0$ (immediately under the A gate) and $y=20$ nm is only about 19%. This may suggest that a separation of 20 nm between adjacent qubit is not enough and an even wider separation is required.

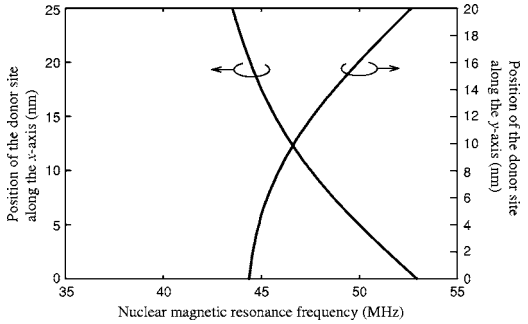

FIG. 9. The variations of the nuclear magnetic resonance frequency with positions of the donor change along the x and y axes. For the variation of the donor site along the x axis, the y and z coordinates of the donor are at 0 and 40 nm, respectively. For the variation of the donor site along the y axis, the x and z coordinates of the donor are at 20 and 40 nm, respectively. The applied static magnetic field $B=2$ T and the other dimensions and parameters are $s=5$ nm, $b=60$ nm, $L=70$ nm, $W=7$ nm, ε_r of silicon=11.46, and ε_r of silicon dioxide=3.9.

IV. CONCLUSIONS

In this paper, we introduced a numerical method to determine the NMR frequency of a donor (^{31}P) doped inside a silicon substrate under the influence of an applied electric field. This phosphorus donor has been suggested for operating as a qubit for the realization of a solid-state scalable quantum computer. Based on the effective-mass theory and the variational method proposed by Ning and Sah,[16] we obtained a set of corrected wave functions for donor. Using the corrected wave functions at the donor site, we formulated a first-order perturbation theory for the perturbed system under the influence of an electric field. In order to calculate the potential distributions inside the silicon and the insulating silicon dioxide layers due to the voltage on the A gate, we used a numerical method to solve an integral equation formulated using the multilayered Green's functions. This enables us to consider arbitrary shape and 3D-structured A gates and the potential distributions can be obtained in an accurate manner. Using this method, we have investigated the potential distributions inside the silicon and silicon dioxide layers. We have also investigated the effects of the thicknesses of silicon and silicon dioxide layers, the relative position of the donor, and the applied gate voltage on the NMR frequency of the donor. Our method provides a potential analysis and design tool for Kane's quantum computer.

APPENDIX A: THE VARIOUS TERMS AND SYMBOLS IN EQ. (14)

The various terms and symbols in Eq. (14) are given as follows:

$$
\begin{aligned}
H_{VA_1A_1} &= \langle \Psi_{A_1}(\mathbf{r})|H_V|\Psi_{A_1}(\mathbf{r})\rangle = \int\int_{V_0}\int \frac{1}{\sqrt{6}}F_{A_1}^{1s^*}(\mathbf{r})\frac{1}{\sqrt{6}}F_{A_1}^{1s}(\mathbf{r})eV(\mathbf{r})[\varphi^*(k_x,\mathbf{r})+\varphi^*(-k_x,\mathbf{r})+\varphi^*(k_y,\mathbf{r})+\varphi^*(-k_y,\mathbf{r})+\varphi^*(k_z,\mathbf{r}) \\
&\quad +\varphi^*(-k_z,\mathbf{r})][\varphi(k_x,\mathbf{r})+\varphi(-k_x,\mathbf{r})+\varphi(k_y,\mathbf{r})+\varphi(-k_y,\mathbf{r})+\varphi(k_z\mathbf{r})+\varphi(-k_z,\mathbf{r})]d\mathbf{r} \\
&\approx \sum_{m=1}^{N}\frac{1}{\sqrt{6}}F_{A_1}^{1s^*}(\mathbf{r}_m)\frac{1}{\sqrt{6}}F_{A_1}^{1s}(\mathbf{r}_m)eV(\mathbf{r}_m)\int\int_{\Omega}\int [\varphi^*(k_x,\mathbf{r})+\varphi^*(-k_x,\mathbf{r})+\varphi^*(k_y,\mathbf{r})+\varphi^*(-k_y,\mathbf{r})+\varphi^*(k_z,\mathbf{r})+\varphi^*(-k_z,\mathbf{r})]\cdot \\
&\quad [\varphi(k_x,\mathbf{r})+\varphi(-k_x,\mathbf{r})+\varphi(k_y,\mathbf{r})+\varphi(-k_y,\mathbf{r})+\varphi(k_z,\mathbf{r})+\varphi(-k_z,\mathbf{r})]d\mathbf{r} \\
&= \sum_{m=1}^{N}\frac{1}{\sqrt{6}}F_{A_1}^{1s^*}(\mathbf{r}_m)\frac{1}{\sqrt{6}}F_{A_1}^{1s}(\mathbf{r}_m)eV(\mathbf{r}_m)\cdot\Omega\cdot 6 = \Omega\sum_{m=1}^{N}F_{A_1}^{1s^*}(\mathbf{r}_m)F_{A_1}^{1s}(\mathbf{r}_m)eV(\mathbf{r}_m),
\end{aligned}
\tag{A1}
$$

where Ω is the volume of the unit cell of silicon, N is the number of unit cells in the silicon layer (volume$=V_0$), and $\mathbf{r}_m$ is the coordinate of the center of the mth unit cell. In simplifying the result in Eq. (A1), we have assumed that the hydrogenic wave function $F_{A_1}^{1s}(\mathbf{r})$ and the potential function $V(\mathbf{r})$ due to the gate voltage are slow-varying functions and almost constant within a unit cell. The Bloch wave functions are orthonormalized as indicated by Kohn.[13] Once the potential $V(\mathbf{r}_m)$ due to the gate voltage is known, Eq. (A1) can be evaluated by numerical summation.

In a similarly way, we have

$$H_{V2sA_1} = \langle \Psi_{2s}(\mathbf{r}) | H_V | \Psi_{A_1}(\mathbf{r}) \rangle \approx \Omega \sum_{m=1}^{N} F_{2s}^{*}(\mathbf{r}_m) F_{A_1}^{1s}(\mathbf{r}_m) eV(\mathbf{r}_m), \tag{A2}$$

$$H_{V3sA_1} = \langle \Psi_{3s}(\mathbf{r}) | H_V | \Psi_{A_1}(\mathbf{r}) \rangle \approx \Omega \sum_{m=1}^{N} F_{3s}^{*}(\mathbf{r}_m) F_{A_1}^{1s}(\mathbf{r}_m) eV(\mathbf{r}_m), \tag{A3}$$

The terms $\langle \Psi_{2s}(\mathbf{r}) | \Psi_{A_1}(\mathbf{r}) \rangle$ and $\langle \Psi_{3s}(\mathbf{r}) | \Psi_{A_1}(\mathbf{r}) \rangle$ in Eq. (14) are independent of the gate voltage and can be evaluated numerically. That is,

$$\begin{aligned} \langle \Psi_{2s}(\mathbf{r}) | \Psi_{A_1}(\mathbf{r}) \rangle &= \langle \Psi_{A_1}(\mathbf{r}) | \Psi_{2s}(\mathbf{r}) \rangle \\ &\approx \sum_{m=1}^{N} \frac{1}{\sqrt{6}} F_{2s}^{*}(\mathbf{r}_m) \frac{1}{\sqrt{6}} F_{A_1}^{1s}(\mathbf{r}_m) \cdot \Omega \cdot 6 \\ &= \Omega \sum_{m=1}^{N} F_{2s}^{*}(\mathbf{r}_m) F_{A_1}(\mathbf{r}_m) \\ &= \int \int \int_{V} F_{2s}^{*}(\mathbf{r}) F_{A_1}^{1s}(\mathbf{r}) d\mathbf{r} = 0.71 \end{aligned} \tag{A4}$$

and

$$\langle \Psi_{3s}(\mathbf{r}) | \Psi_{A_1}(\mathbf{r}) \rangle = \langle \Psi_{A_1}(\mathbf{r}) | \Psi_{3s}(\mathbf{r}) \rangle \approx 0.27. \tag{A5}$$

The ground-state energy E_{A_1} in Eq. (14) is obtained by the variation method (Ning and Sah[16]) and is equal to 45.47 meV with respect to the conduction band minimum. The excited energies E_2 and E_3 are calculated as hydrogenic energy levels with a Bohr radius given by Eq. (10). Their values are 7.5 meV and 3.3 meV, respectively, with respect to the conduction band minimum.

APPENDIX B: THE GREEN'S FUNCTIONS FOR THE SILICON AND SILICON-DIOXIDE QUBUIT STRUCTURE

The Green's functions listed here are for a three-layered structure with the source placed in the interface between the second and third layers. Layer 1 is the silicon substrate, layer 2 is the insulating layer of silicon dioxide, and layer 3 is the space above the silicon dioxide layer. The field coordinates (x,y,z) and the source coordinates (x',y',z') are referring to local coordinate systems within each layer.[24] The various Green's functions are expressed in terms of a spectral domain kernel, which can be numerically approximated by using Prony's method, and the spatial Green's function are obtained by using the complex image method.[22] The three-layered Green's functions are listed below.

$$\begin{aligned} G_{13}(x,y,z|x',y',z') = \frac{1}{(2\pi)^2} \int_{-\infty}^{\infty} \int_{-\infty}^{\infty} \tilde{G}_{13}(k_x,k_y,z,z') \\ \exp[-jk_x(x-x')] \\ \times \exp[-jk_y(y-y')] dk_x dk_y, \end{aligned} \tag{B1}$$

where the spectral domain kernel is

$$\gamma = \sqrt{k_x^2 + k_y^2}, \quad \tilde{G}_{13}(k_x,k_y,z,z') = \left(\frac{1}{\varepsilon_0 \gamma}\right) \frac{\dfrac{\varepsilon_{r2} \sinh(\gamma z)}{\sinh(\gamma h_1)\sinh(\gamma h_2)}}{\varepsilon_{r2}\varepsilon_{r3} + \varepsilon_{r2}\varepsilon_{r3} \coth(\gamma h_2) + \varepsilon_{r1}\varepsilon_{r3} \coth(\gamma h_1) + \varepsilon_{r1}\varepsilon_{r2} \coth(\gamma h_1)\coth(\gamma h_2)}, \tag{B2}$$

where $G_{13}(x,y,z|x',y',z')$ is the Green's function representing the potential inside layer 1 due to a unit charge in layer 3. The other two Green's functions are

$$G_{23}(x,y,z|x',y',z') = \frac{1}{(2\pi)^2} \int_{-\infty}^{\infty} \int_{-\infty}^{\infty} \tilde{G}_{23}(k_x,k_y,z,z') \exp[-jk_x(x-x')] \exp[-jk_y(y-y')] dk_x dk_y, \tag{B3}$$

where

$$\tilde{G}_{23}(k_x,k_y,z,z') = \left(\frac{1}{\varepsilon_0 \gamma}\right) \frac{\dfrac{\varepsilon_{r1} \coth(\gamma h_1)\sinh(\gamma z) + \varepsilon_{r2} \cosh(\gamma z)}{\sinh(\gamma h_2)}}{\varepsilon_{r2}\varepsilon_{r3} + \varepsilon_{r2}\varepsilon_{r3} \coth(\gamma h_2) + \varepsilon_{r1}\varepsilon_{r3} \coth(\gamma h_1) + \varepsilon_{r1}\varepsilon_{r2} \coth(\gamma h_1)\coth(\gamma h_2)}. \tag{B4}$$

Finally, the Green's function representing the potential inside layer 3 due to a unit charge in layer 3 is given by,

$$G_{33}(x,y,z|x',y',z') = \frac{1}{(2\pi)^2}\int_{-\infty}^{\infty}\int_{-\infty}^{\infty}\tilde{G}_{33}(k_x,k_y,z,z')\exp[-jk_x(x-x')]\exp[-jk_y(y-y')]dk_x dk_y, \tag{B5}$$

where

$$\tilde{G}_{33}(k_x,k_y,z,z') = \left(\frac{1}{\varepsilon_0\gamma}\right)\frac{\varepsilon_{r1}\coth(\gamma h_1)+\varepsilon_{r2}\coth(\gamma h_2)}{\varepsilon_{r2}\varepsilon_{r3}+\varepsilon_{r2}\varepsilon_{r3}\coth(\gamma h_2)+\varepsilon_{r1}\varepsilon_{r3}\coth(\gamma h_1)+\varepsilon_{r1}\varepsilon_{r2}\coth(\gamma h_1)\coth(\gamma h_2)}. \tag{B6}$$

With these Green's functions, the charge distribution $Q(x',y')$ on the strip and the A gate due to a unit voltage on strip and the A gate can be obtained by solving the following integral equation using the moment method:[21]

$$1 = \int\int_S G_{33}(x,y,0|x',y',0)Q(x',y',z')dx'dy', \tag{B7}$$

where S is the area of the strip and the A gate. Once $Q(x',y')$ is known, the potentials due to a 1 V voltage on the strip and the A gate can be evaluated as

$$V_{13}(x,y,z) = \int\int_S G_{13}(x,y,z|x',y',0)Q(x',y')dx'dy', \quad \text{in layer 1} \tag{B8}$$

$$V_{23}(x,y,z) = \int\int_S G_{23}(x,y,z|x',y',0)Q(x',y')dx'dy', \quad \text{in layer 2} \tag{B9}$$

$$V_{33}(x,y,z) = \int\int_S G_{33}(x,y,z|x',y',0)Q(x',y')dx'dy', \quad \text{in layer 3}. \tag{B10}$$

[1] M. A. Nielsen and I. L. Chuang, *Quantum Computation and Quantum Information* (Cambridge University Press, Cambridge, England, 2000), and the references therein.
[2] N. A. Gershenfeld and I. L. Chuang, Science **275**, 350 (1997).
[3] D. G. Cory, M. D. Price, and T. F. Havel, Physica D **120**, 82 (1997).
[4] B. E. Kane, Nature (London) **393**, 133 (1998).
[5] G. P. Berman, D. K. Campbell, G. D. Doolen, and K. E. Nagaev, J. Phys.: Condens. Matter **12**, 2945 (1999).
[6] K. A. Valiev and A. A. Kokin, quant-ph/9909008 (unpublished).
[7] D. Loss and D. P. DiVincenzo, Phys. Rev. A **57**, 120 (1998).
[8] T. Schenkel, A. Persaud, and S. J. Park, J. Appl. Phys. **94**, 7017 (2003).
[9] C. J. Wellard and L. C. L. Hollenberg, Phys. Rev. B **72**, 085202 (2005).
[10] J. M. Luttinger and W. Kohn, Phys. Rev. **97**, 869 (1955).
[11] W. Kohn and J. M. Luttinger, Phys. Rev. **97**, 883 (1955).
[12] W. Kohn and J. M. Luttinger, Phys. Rev. **98**, 915 (1955).
[13] W. Kohn, in *Solid State Physics*, edited by F. Seitz and D. Turnbull (Academic Press, New York, 1957), Vol. 5, p. 257.
[14] R. A. Faulkner, Phys. Rev. **184**, 713 (1969).
[15] A. Baldereschi, Phys. Rev. B **1**, 4673 (1970).
[16] T. H. Ning and C. T. Sah, Phys. Rev. B **4**, 3468 (1971).
[17] S. T. Pantelides and C. T. Sah, Phys. Rev. B **10**, 621 (1974).
[18] A. A. Larionov, L. E. Fedichkin, A. A. Kokin, and K. A. Valiev, Nanotechnology **11**, 392 (2000).
[19] L. M. Kettle, H. S. Goan, S. C. Smith, C. J. Wellard, L. C. L. Hollenberg, and C. I. Pakes, Phys. Rev. B **68**, 075317 (2003).
[20] B. Koiller, X. Hu, and S. DasSarma, Phys. Rev. B **66**, 115201 (2002).
[21] R. F. Harrington, *Field Computation by Moment Methods* (IEEE Press, New York, 1993).
[22] Y. L. Chow, J. J. Yang, and G. E. Howard, IEEE Trans. Microwave Theory Tech. **39**, 1120 (1991).
[23] R. C. Fletcher, W. A. Yager, G. L. Pearson, A. N. Holden, W. T. Read, and F. R. Merritt, Phys. Rev. **94**, 1392 (1954).
[24] K. Li, K. Atsuki, and T. Hasegawa, IEEE Trans. Microwave Theory Tech. **45**, 2 (1997).
[25] T. Itoh, R. Mittra, and R. D. Ward, IEEE Trans. Microwave Theory Tech. **20**, 847 (1972).
[26] S. Yoon and M. White, J. Electron. Mater. **19**, 487 (1999).